5-2014

Assessing Layer Parallel Shortening in the Eastern Colorado Front Range Using Thin Section Analysis and Analog Sandbox Models

Nicole Pierson
University of Nebraska-Lincoln, nicole_pierson2000@yahoo.com

Assessing Layer Parallel Shortening in the Eastern Colorado Front Range Using Thin Section Analysis and Analog Sandbox Models

by

Nicole Pierson

A THESIS

Presented to the Faculty of

The Graduate College at the University of Nebraska

In Partial Fulfillment of Requirements

For the Degree of Master of Science

Major: Earth and Atmospheric Sciences

Under the Supervision of Professor Caroline M. Burberry

Lincoln, Nebraska

May, 2014

Assessing Layer Parallel Shortening in the Eastern Colorado Front Range Using Thin Section Analysis and Analog Sandbox Models

Nicole Pierson, M.S.

University of Nebraska, 2014

Adviser: Caroline M. Burberry

Layer parallel shortening (LPS) is an expression of compressive strain that occurs parallel to bedding surfaces. LPS is chiefly expressed by chemical changes to sediment volume, including stylolitization, porosity reduction and impingement of grains. This strain is typically omitted in the process of cross-section restoration due to a lack of understanding of spatial and temporal LPS accommodation. Bulk shortening calculated is considered to be a minimum shortening estimate. However, dismissing this inaccuracy due to shortening can lead to significant error in subsurface predictions and reconstructions.

To address this problem, a combination of thin section analysis and analog modeling assessed the amount of LPS across the central Colorado Front Range (CFR) system. A geologic cross-section of the eastern CFR was built using field data and a minimum bulk shortening was calculated. A scaled analog model was deformed incrementally in accordance with the cross-section restoration and Colorado's well-constrained tectonic history. Cross-sections from the model were restored and compared to the cross-section of the CFR.

LPS results from the analog model and from thin sections show a complex relationship between LPS and geologic setting. LPS is variable with respect to depth in the stratigraphic column, with respect to divisions of mechanical strength in the stratigraphy, and in proximity to meso- and macroscale structures. Thus, there is no single rule for spatial and temporal LPS accommodation that can be applied to any deformed belt. LPS needs to be treated separately in each stratigraphic or mechanical unit and varies with increasing distance from major structural features such as faults. LPS is measurable, and can be addressed with strategic sampling using oriented core in any region dominated by sandstone and limestone.

Dedication

This thesis is dedicated to the late Kathryn Colleen Gallagher, whose witty humor and loving support the author still cannot imagine going without.

Acknowledgements

I would like to thank the people and organizations that made this research possible. First and foremost I would like to thank my family: Megan, Beth, John and Steven, whose unwavering support from beginning to end of this project has kept me on track, and my friends, whose moral support helped me to achieve my goals. I would like to thank my adviser Dr. Caroline M. Burberry for her expertise, support, and occasionally her shoulder through both my undergraduate and graduate experiences. Also deserving of recognition are my lab mate Matthew Peppers for his assistance with my lab work when I didn't have enough arms, and his unwavering upbeat attitude; Shelby Chandler for her assistance in the field; the Department of Earth and Atmospheric Sciences at the University of Nebraska-Lincoln for providing me with financial support and the opportunity to research alongside esteemed faculty; Dr. David Watkins and Dr. Christopher Fielding for serving on my committee; Midland Valley Ltd. for providing an academic license for software used in this project; the UNL AAPG Student Chapter for electing me to serve on their leadership board alongside my best friend. Thank you.

Table of Contents

Multimedia Objects Table of Contents

Introduction

Layer parallel shortening (LPS) is an expression of compressive strain that occurs parallel to bedding surfaces, including both mechanical and chemical changes; it is dependent on many factors, such as rock mechanics and amount of stress applied (Fischer and Coward, 1982; Laubach, 1997). Typically, this deformation is not incorporated into cross-section restoration. Although an amount of bulk shortening can be calculated, internal deformation is usually ignored in part because the amount and location of shortening increments is unknown (Sans et al., 2003). Specific questions addressed in this contribution are: is LPS only accommodated at the onset of deformation? Is it accommodated throughout the deformation sequence? Is the amount of LPS consistent with increasing depth in the stratigraphic column? Does the amount of LPS vary with distance from mesoscale and macroscale structures? By ignoring the error generated by disregarding LPS, palinspastic reconstructions are fundamentally flawed – a step in the restoration is missing. LPS is necessary to area-balance a cross-section, is responsible for volume changes within beds, and can be accommodated in multiple structural forms (Epard and Groshong, 1995). Thus, current subsurface predictions are not taking into account all expressions of deformation. This leads to poor predictive capability with regards to fluid flow trajectories, trap volume, trap location, porosity and permeability. LPS does not solely reveal itself in cross-section restoration; calcite twins, intracrystalline deformation, cataclastic flow between grains or via fracturing, grain impingements, fracturing, and stylolite formation can all be measured for LPS. Accordingly, this study uses a combination of field measurements and thin section analysis to calculate the

amount of LPS across the central Colorado Front Range (CFR) to address the four questions listed above.

Geologic Setting

The CFR is contained within the North American Rocky Mountains, recognized as the most well-known Precambrian-bearing mountain range (Jordan and Allmendinger, 1986). It marks the easternmost extent of the Rocky Mountains, and has been influenced by multiple cycles of deformation. North-Northwest faulting took place in the Mesoproterozoic; these faults were subsequently reactivated during the Pennsylvanian-Permian Ancestral Rocky Mountain uplift and the Late Cretaceous-Eocene Laramide Orogeny (Tweto, 1980a). The CFR currently lies in the intraplate region of the North American plate, and is defined as the highland east of the Sawatch Range, west of the Denver Basin, and between 38ºN and 41ºN in the state of Colorado (Tweto, 1980c). This study focuses on the eastern portion of the Colorado Front Range from the crystalline basement out into the Denver Basin (Figure 1).

The CFR has had a complex history, spanning almost two billion years. The oldest rock unit in the study area is the metamorphic Idaho Springs Formation, which is Paleoproterozoic and metamorphosed at about 1.75 Ga (Figure 2; Hedge et al., 1967). Its protolith has been interpreted as one of multiple oceanic volcanic arcs and related sedimentary basins that developed off the southern edge of the Archean Wyoming craton (Tweto, 1980a). This complex was welded to the Wyoming craton between 1.74 and 1.69 Ga in the Yavapai-Mazatzal orogeny (Jessup et al., 2006). The CFR provides the largest continuous exposure of the Yavapai-Mazatzal province recorded in Colorado's

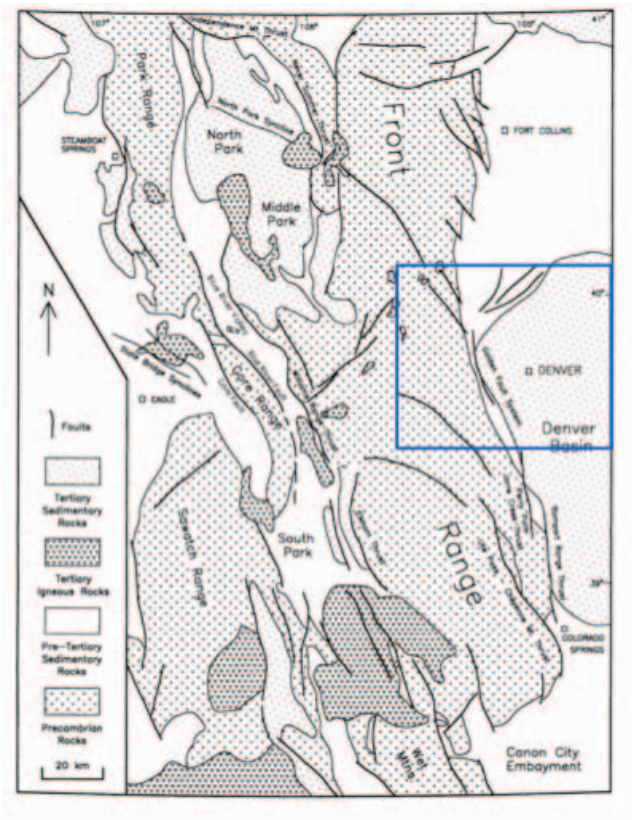

Figure 1: Generalized map of the Colorado Front Range, outlining the study area in blue; modified from Erslev et al., 1999.

Proterozoic metamorphic units (Smith et al., 1999). From the Proterozoic to Pennsylvanian, the CFR was tectonically quiescent, affected only by waxing and waning sea levels (Oldow et al., 1989). From the Pennsylvanian to the Permian, the Ancestral Rocky Mountains (ARM) formed basement-involved arches and structural highs bounded by thrust faults, including what became the CFR (Figure 2; Kluth and Coney, 1981; Barbeau, 2003). ARM deformation is probably the result of the suturing of the North and South American plates during the assembly of Pangea, which was completed in the Permian (Ross, 1979). This broad intraplate deformation caused enough uplift for significant erosion, and the resultant alluvial fan deposit, the Fountain Formation, is about 3,000 feet (914 meters) thick in the study area (Sweet and Soreghan, 2010). In the Mesozoic, thin-skinned Sevier orogenic deformation began in the Middle Jurassic west of the study area; however, far field stresses are expected to have affected the study area (Oldow et al., 1989). From the late Albian to Maastrichtian, the study area was covered by the Western Interior Seaway (Kauffman, 1984). During inundation, the study area was covered in a thick deposit of

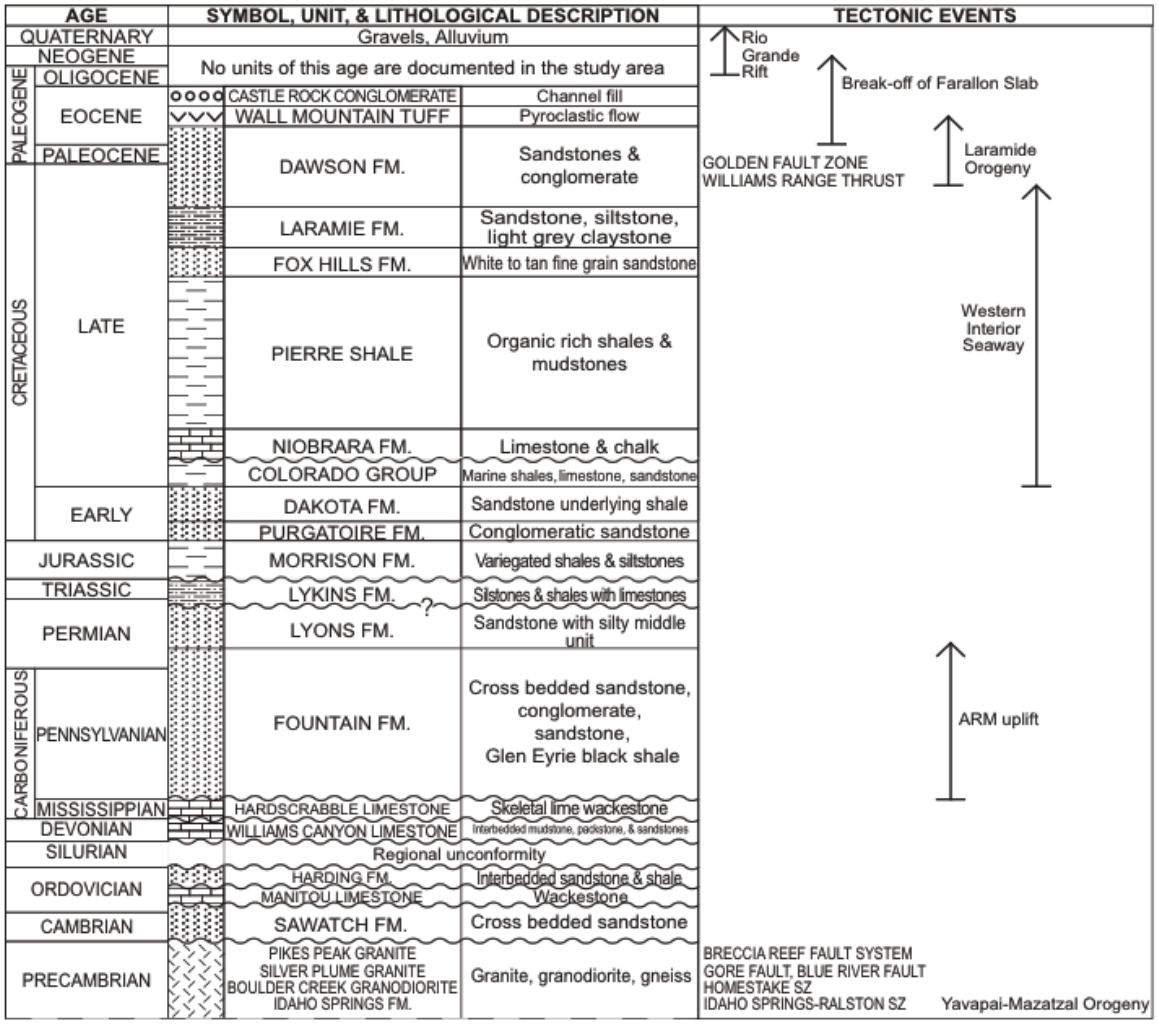

Figure 2: Tectonostratigraphic column of formations present within the study area. Not to scale. Compiled by the author and from references within the text.

organic-rich mud at a high sedimentation rate: the Pierre Shale (Figure 2; Weimer and Le Roy, 1987). This unit ranges from about 3,300 to 5,000 feet (1006 meters to 1524 meters) thick; the thickest formation in the study area (Grose, 1972). The study area was not uncovered by the sea until the final regression of the Seaway, as the Sevier orogeny transitioned into the Laramide orogeny (Kauffman, 1984; Humphreys, 2009). The Laramide orogeny stands out as a period of extensive deformation due to flat slab

subduction, characterized by strong, intraplate tectonism (Tweto, 1980b). The Laramide orogeny is diachronous; it began in the study area between 70 to 65 Ma, and concluded in the Eocene, at about 40 Ma (Figure 2; Tweto, 1980b). Faults from the ARM uplifts were reactivated and overprinted during this orogeny (Barbeau, 2003). Due to the Laramide mountain-building event and subsequent erosion, Precambrian rocks now occupy nearly 12 percent of Colorado's surface area (Tweto, 1980a). Post Laramide Orogeny, it has been suggested that study area continues to be regionally uplifted (Steven et al., 1997).

For the purposes of this study, the stratigraphic column has been subdivided into mechanically similar packages. Mechanical stratigraphy subdivides rock units by physical properties such as brittleness and tensile strength (Laubach et al., 2009). In the area where the cross-section was drawn, the Cambrian to Pennsylvanian units are not present (Figure 3). Consideration of the Permian to Paleocene sequence shows that the Pierre Shale is a significant ductile unit in the area. The stratigraphic column in the study area can thus be divided into dominantly brittle Permian to Late Cretaceous units, ductile Late Cretaceous Pierre Shale, and brittle Late Late Cretaceous to Paleocene units. These divisions are used in Figures 3 and 4 and in scaling the analog model.

Methods

Oriented hand samples from the sedimentary section of the study area were collected for thin section analysis. Only sandstone and limestone hand samples whose strike and dips were directly measurable (i.e. only in situ outcrop qualifies) were collected. Error in sample orientation is thought to be less than 5º (Chapple and Spang, 1974).

A geologic cross-section was constructed west to east across the study area for two reasons: to obtain a shortening amount from the restored section for use in the analog models and to compare and contrast with final model geometries. Strike and dip measurements and fault orientations recorded in the study area were used when constructing the cross-section (Figure 3). Bose and Mitra (2010) found that the complexities of listric normal faults cannot be seen in the analog model scale, so only large-scale faults were mapped and smaller-scale secondary faults were not included. The resultant cross-section is modified from Kellogg et al. (2004) using field measurements (Figure 3).

Since the goal of modeling is to represent a scaled-down version of natural upper-crustal conditions by observing geometric and dynamic relationships, the constructed cross-section, Figure 3, was restored (Figure 4). Restoration of the cross-section assumed plane strain, constant volume, constant line length, constant unit thickness, and a negligible loading effect. The loading effect assumption was used because the model was not compacted before it was run. The goals of the restoration were to elucidate how many deformation phases needed modeling, to get a sense of the deformation progression in the area, and to calculate the amount of shortening. The irregular basal surface seen in Figure 4 represents the irregular basement topography at the time of deposition of the overlying Pennsylvanian-Permian Fountain Formation. The restored cross-section displays two dominant deformation events (Figure 4). Minimum shortening values calculated are 17.5% pre-Pierre Shale shortening, and 9.01% deformation in the post Pierre Shale units using Equation 1 and the rigid beam assumption. The Dakota Formation, which forms

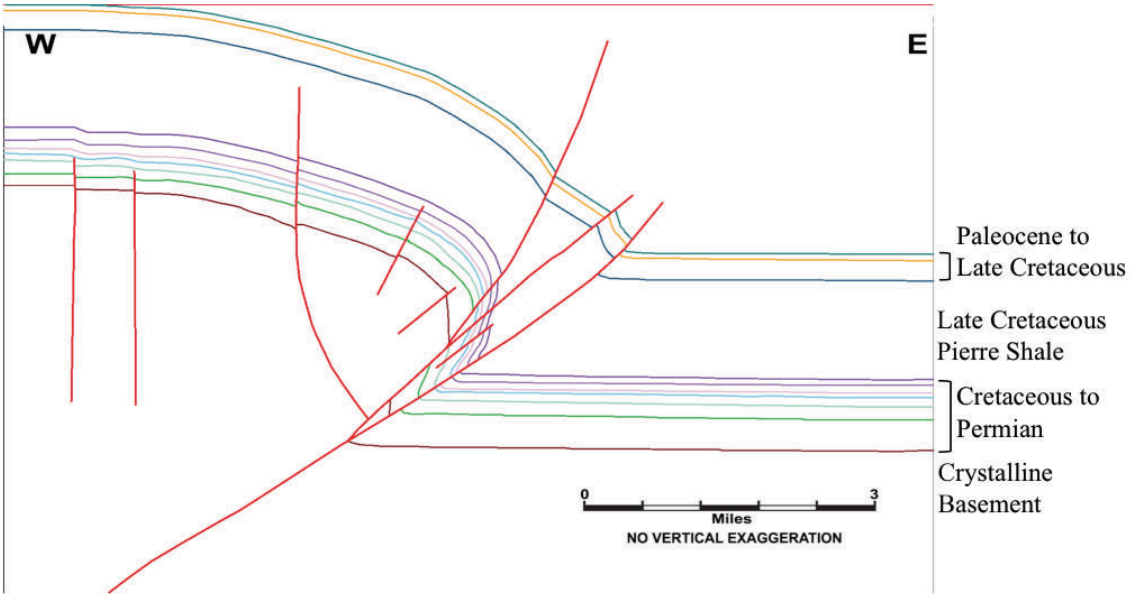

Figure 3: Cross-section across the eastern portion of the Colorado Front Range modified from Kellogg et al., 2004. Faults are in red. Stratigraphic units divided by mechanical properties are labeled on the right.

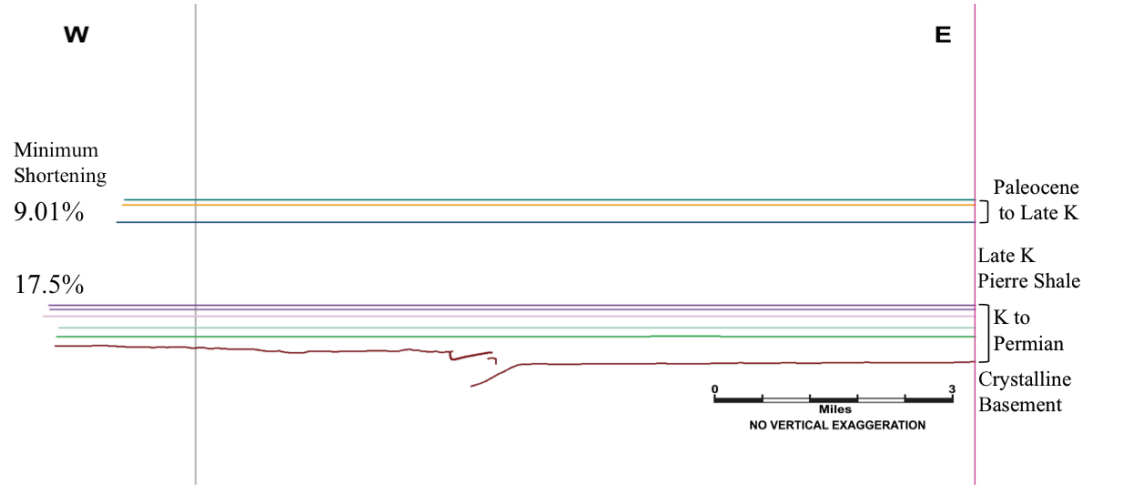

Figure 4: Colorado Front Range cross section from Figure 3 restored back to flat; minimum shortening for each mechanical package (pre- and post Pierre Shale) was calculated by bed length changes and is reported on the left.

$$e = \frac{\ell - \ell_0}{\ell_0} \cdot 100\%$$

Equation 1: Percent shortening calculation where ℓ is the length measured and ℓ_0 is the original length.

prominent hogbacks in the field, was assumed to be a rigid stratigraphic unit (Figure 2). These numbers, combined with the geometries mapped in cross-section, were used to construct and deform the analog sandbox model.

Thin Section Analysis

In this study, oriented thin sections provide insight into how layer-parallel diagenetic processes such as compaction and pressure solution account for volume loss by examining directional grain dissolution. Thin section analysis was carried out using the Onasch (1993) method for calculating pressure solution shortening. This calculates directional grain dissolution from diagenetic compaction and LPS. A representative photomicrograph of each oriented thin section was taken in plane-polarized, cross-polarized light, or using a gypsum plate for maximum contrast at grain boundaries. Photographs were taken using a petrographic microscope and an Olympus microscope-specific camera utilizing cellSens software. Each photograph oriented the dip direction left-right and the compaction direction up-down. Best fit ellipses were drafted around grains onto one photomicrograph per sample based on sharpness of grain boundaries. Where best fit ellipses crossed, the Onasch (1993) method was applied. At least 50 of this type of grain contact were measured per thin section image. In the Onasch (1993) method, the orientation of the compromise boundary, Line X-Y, determines the

orientation of an orthogonal line through the center of X-Y representing the direction of stress applied (Figure 5a). Points C and D are along this orthogonal line at the inferred grain boundary pre-pressure solution shortening (the dashed lines; Figure 5a). Points A and B mark the center point of the ellipse from C or D respectively to the edge (Figure 5a). These points are then used to calculate e, or percent shortening (Equation 2):

$$e = \frac{AB - (AB + CD)}{AB + CD} \cdot 100\%$$

Equation 2: From Onasch, 1993.

The percent shortening e is plotted with the orientation orthogonal to the compromise boundary on a stereonet (Figure 5b). It is then used to calculate the compaction percentage and LPS percentage by measuring the distance from a best fit circle through all 50+ plotted boundaries to the edge of the stereonet. LPS is represented by the distance from the edge of the stereonet to the best fit circle on the side, and compaction is measured by that same distance but from the top or bottom.

Analog Modeling

Compressive deformation has been studied with scaled experiments since the 1800s (Cadell, 1888; Schreurs et al., 2006; Buiter, 2012). The University of Nebraska-Lincoln Earth and Atmospheric Sciences Deformation Research Group uses a glass-walled analog model with a motorized straight, rigid moving wall. Models were not precompacted. The moving wall compresses at about 10 millimeters per hour. Materials used include dry, well-sorted, well-rounded coarse and fine sand fractions as well as a Xiameter silicone polymer RBG-0901 produced by the Dow Corning Corporation. The

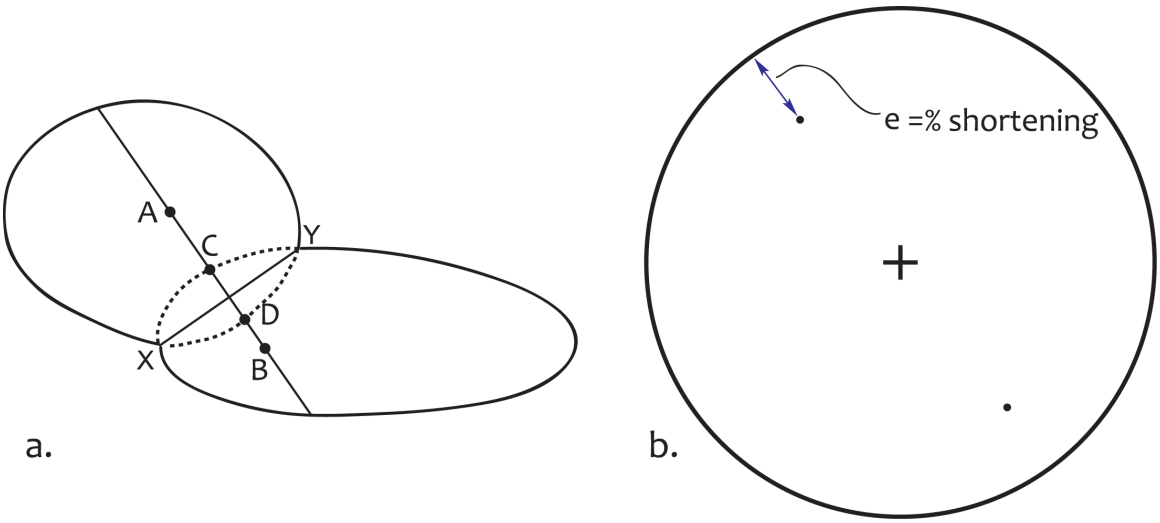

Figure 5: Modified from Onasch, 1993.
5a. Two grains which have been compressed together. The dashed lines represent the inferred boundaries of the grains pre-compression. Line XY is the compromise boundary. Points A, B, C, and D lie along a line perpendicular to the compromise boundary.
5b. A stereonet displaying line e, percent shortening, plotted with the azimuth direction of the line perpendicular to the compromise boundary from Part a. e is calculated using Equation 2.

length ratio of the model was such that 0.5 model centimeters was equivalent to 5,000 feet (1524 meters), so that the tectonostratigraphic column, Figure 2, could be simplified into four units based on formation thicknesses and mechanical properties (Figure 6).

Scaling. Mechanical stratigraphy in sandbox models has been shown to play a key role in controlling the deformation style and timing, so it was critical that the CFR and model were scaled properly (Turrini et al., 2001). The scenario modeled is a scaled depiction of the CFR following within principles of geometric, rheological, and dynamic similarity (Hubbert, 1937; Withjack and Schlische, 2006; Cerca et al., 2010). To satisfy the requirement for dynamic similarity, physical properties of both the natural and analog materials must be similar so that forces, stresses and strengths are scaled the same

amount; for example, the coefficient of internal friction of both materials must be equal to or close to the modeled rock value (Hubbert, 1937). The coefficient of internal friction of upper crustal rocks is reported to be 0.85 (Byerlee, 1978; Weijermars, 1992; Koyi and Petersen, 1993). Cohesion was measured in the laboratory using a simplified Hubbert-type shear box (Hubbert, 1951). The coefficient of internal friction of loose model sand was measured to be 0.59 for fine sand and 0.99 for coarse sand by measuring normal and shear stresses in the laboratory (Schellart, 2000). Cohesion similarity for the two materials is calculated using the relationship of density, length scaling factor and gravity with shear stress, given by the ratio ($\rho lg/\tau_{0)}$ where ρ represents density, l is the length, g is acceleration due to gravity, and τ_0 is the coefficient of cohesion (Table 1.1; Nilforoushan and Koyi, 2007). The two non-dimensional ratio ranges are 0.635-0.985 for nature and .0599 -0.0617 for the lab setting, respectively (Table 1.1). This suggests that the model fulfills the criterion for dynamic scaling.

In the case of geometric similarity, in sand models major faults accommodate the majority of hanging wall deformation in a narrow zone (Withjack and Schlische, 2006). In models utilizing wet clay, many minor faults accomodate the majority of hanging wall deformation (Withjack and Schlische, 2006). Though they produce similar fault patterns, the lower cohesion and larger grain size of sand when compared to clay is favorable when modeling the CFR (Buiter, 2012). The coefficient of internal friction for dry sand is less than that of wet clay (Bose and Mitra, 2010). Both materials have scalable cohesive strengths on the order of ~10^{-4} to 10^{-5} of upper crustal rock (Hubbert,

Table 1.1: Scaling parameters for Colorado Front Range model

Quantity	Nature	Model	Scaling Ratio
Acceleration due to gravity (m/s^2)	9.81	9.81	$a_m/a_n = 1$
Thickness: upper brittle unit	5882 ft	0.5 cm	$L_m/L_n = 0.85$
Thickness: ductile unit	5000 ft	0.5 cm	$L_m/L_n = 1$
Thickness: lower brittle unit	4850 ft	0.5 cm	$L_m/L_n = 1.03$
Density: brittle units	2.2-2.8 g /cm^3	1.76 g/cm^3	$\rho_m/\rho_n = 0.8\text{-}0.63$
Density: brittle basement	2.7 g/cm^3	1.71 g/cm^3	$\rho_m/\rho_n = 0.63$
Density contrast	0.1-0.5 g/cm^3	0.05 g/cm^3	$\rho_m/\rho_n = 0.1\text{-}0.5$
Friction coefficient (brittle overburden units)	0.85	0.59	0.69
Friction coefficient (brittle basement)	0.85	0.99	0.14
Viscosity of ductile unit	3.8×10^6 Pa·s *	5×10^5 Pa·s	0.13
Cohesion coefficient	5,000,000 Pa ~	140 Pa ~	2.8×10^5
$\rho lg/\tau_0$ ratio	0.77	0.61	0.0608-0.0971
Shortening Rate	0.011 cm/yr	8.76×10^3 cm/yr	7.96×10^5

* Ricker, 1941
~ Nilforoushan and Koyi, 2007

1937; Bose and Mitra, 2010). Analog models with sand and silicone have been shown to successfully model Laramide deformation (Cerca et al., 2010).

Model Setup. The restored cross-section displays two dominant deformation events, with calculated minimum shortening values of 17.5% for the pre-Pierre Shale deformation sequence, and 9.01% for the post Pierre Shale deformation sequence (Figure 4). These values were used to help constrain the deformation of the model. Based on the two deformation phases gleaned from the CFR cross-section, the model was run in two stages. In the first deformation phase, the basement and sedimentary section up to the Pierre Shale were deposited flat (Figure 6). A straight fault was cut into the model parallel to the moving wall, representing the basin-bounding reactivated fault from the cross-section in Figure 3 (Figure 7). These two basal layers were deformed 7.85%, based on the geometry viewed in the glass wall during deformation. After the first deformation phase, the sedimentary section was completed by the addition of the ductile silicone polymer representative of the Pierre Shale and the uppermost fine sand layer (Figure 6). The silicone polymer was laid down as a prepared 0.5 centimeter thick sheet. It has been shown that as long as the analog model deformation front does not reach the edge of the silicon sheet, the model responds as if the sheet is

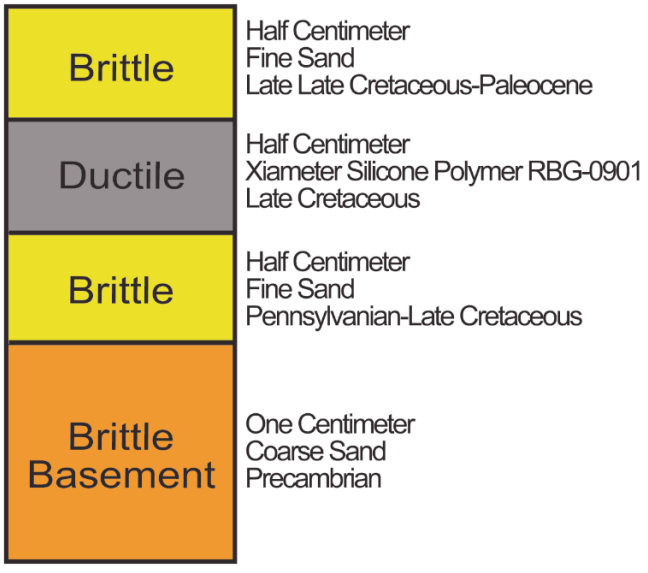

Figure 6: Stratigraphic column of the Colorado Front Range sandbox model.

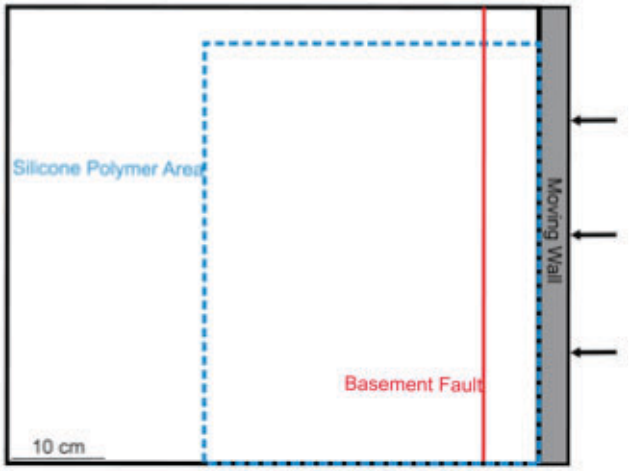

Figure 7: Setup diagram of the sandbox Colorado Front Range model run with the rigid moving wall on the right in grey, the basement fault cut in red, and the original outline of the silicone polymer in a blue dashed pattern.

infinite (Burberry et al., in press). Continental deformation decays exponentially from the collisional margin, in this case, the moving wall; and the model was scaled such that the deformation would not propagate to the edge of the sheet (Craddock et al., 1993). The model was then deformed an additional 9.7%, for a total of 17.55% bulk shortening. During the whole of the model run, photographs of the top surface and cross-section were taken about every hour. After the model run finished, it was immediately sandpacked with a minimum of three centimeters of sand so that the silicone polymer would not flow out of the structures created. The model was then wet with a combination of water and dish soap, both by injecting water into the layers and by spraying at the surface of the model. Once wet, the model was sliced perpendicular to the compression direction (parallel to dip) and cleaned using a long, heated knife every centimeter where possible. A photograph through the side glass viewing wall was taken at every slice. These photographs were used in the restoration of model cross-sections, which will be discussed in a subsequent section (see Figure 11).

Thin Section Analysis Results

Four quartz arenites used in the analysis were collected from the eastern side of the Colorado Front Range (Figure 8). Samples NP6 and NP2 are from the Late Cretaceous Laramie Formation. Sample CB3 is from the Early Cretaceous Dakota Formation, and CB6 is from the Jurassic Morrison Formation near the Dakota-Morrison contact. An example of the Onasch (1993) method on sample CB3 is below (Figure 9). For other thin section measurements, see Appendix A. Sample CB3 has 17.9% LPS and 15.9% compaction (Table 1.2). Sample CB6 has 12.1% LPS and 10.2% compaction (Table 1.2). Sample NP2 measures 27.8% LPS and 21.0% compaction – the highest amount of all four samples (Table 1.2). The lowest amount measured is from sample NP6, which displays an LPS amount of 11.6% and 9.5% compaction (Table 1.2).

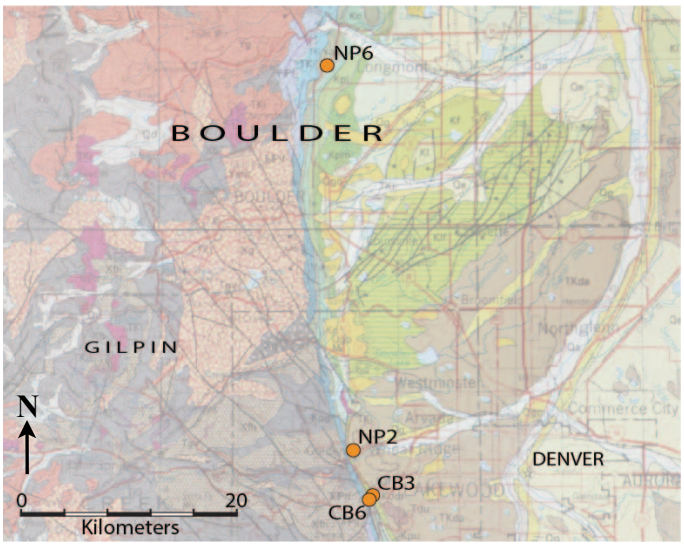

Figure 8: Location map showing the locations of the hand samples collected with orange dots. Reds, greys, and patterned formations are crystalline. The sedimentary section is represented by browns (Tertiary), greens (Cretaceous), blues (Pennsylvanian-Triassic), and yellow (Quaternary). Basemap modified from Tweto, 1979.

a.

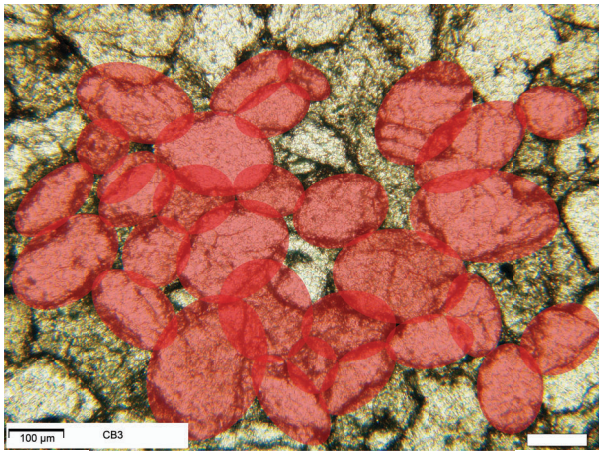

b.

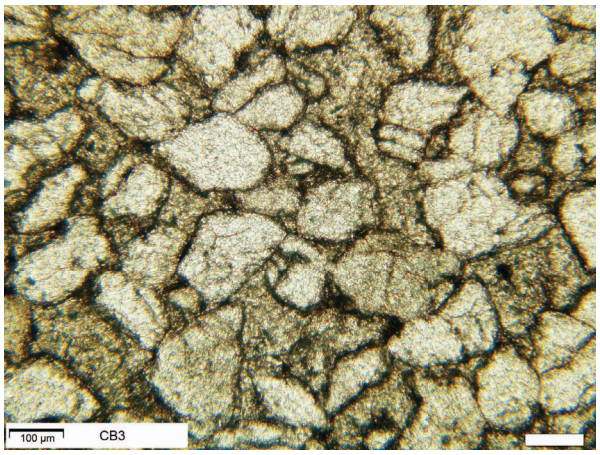

c.

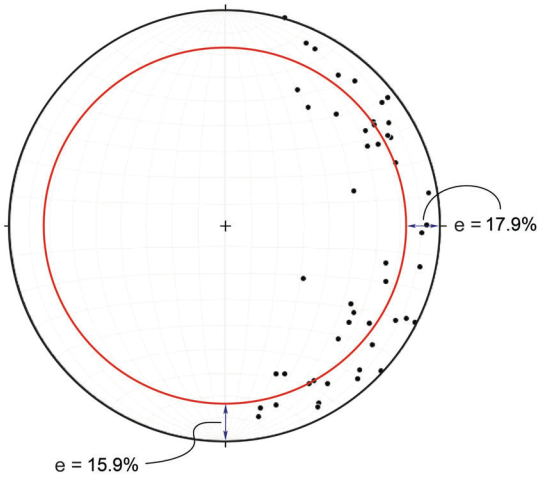

Figure 9: Analysis of sample CB3 utilizing the Onasch (1993) method.
a. Photomicrograph under plane-polarized light.
b. Photomicrograph with best fit ellipses drafted on.
c.S tereonetof pl ottedl ayerpa rallels horteninga nd compaction directions.

Table 1.2: Field sample LPS values calculated using the Onasch (1993) method.

Sample	LPS %	Compaction %
CB3	17.9	15.9
CB6	12.1	10.2
NP2	27.8	21
NP6	11.6	9.5

Analog Modeling Results

At the final stage of bulk shortening, a series of thrust faults had formed along the deformation front, many of which are discontinuous in map view, particularly in the foreland (Figure 10). Each cross-section of the model cut was assigned a number based on how far it was sliced from the glass viewing wall. The three cuts that were restored are 12, 18 and 24 centimeters, respectively (Figure 10). Analog model cross-section restoration utilized Midland Valley Move software. Horizons from cross-section

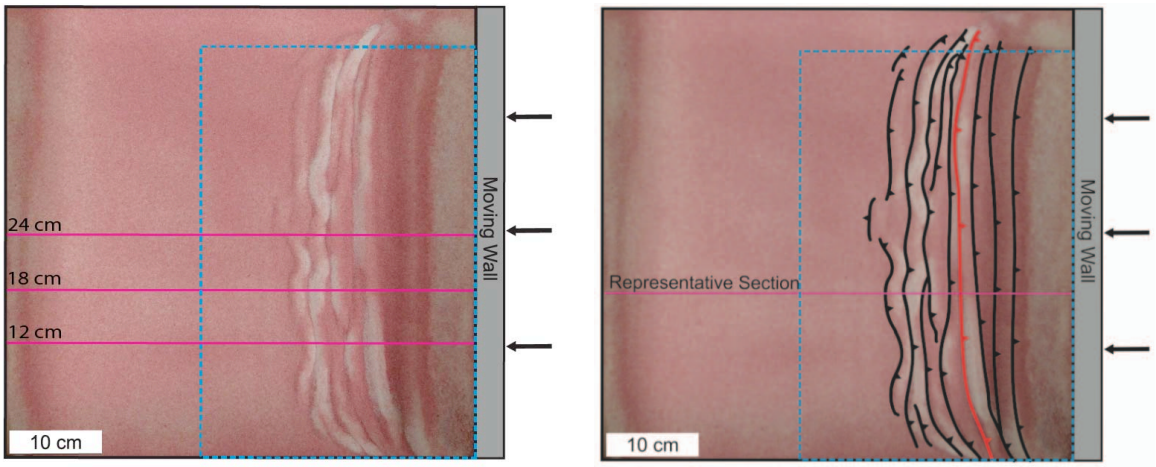

Figure 10: Top view of analog model after 17.55% bulk shortening; uninterpreted (left) and interpreted (right); the blue patterned box represents the extent of the silicone polymer, the fault in red represents the surface expression of the basement fault cut, and the section lines in pink mark the surface point of the vertical model slices of Figure 11.

photographs were traced over and faults were interpreted (Figure 11a; Figure 11b). Displacement along faults was removed. Lastly, beds were flattened by maintaining constant thickness (Figure 11c). Minimum layer parallel shortening of each bed was calculated by taking the length difference from each horizon to the original back wall and accounting for sand lost from the underside of the moving wall (Equation 1). This is represented by the red polygons in Figure 11c. The sand volume lost from below the moving wall was almost negligible, accounting for no more than 0.006% of total volume of sand in the model. This LPS amount was then subtracted from the bulk shortening amount to calculate the shortening from faulting and folding. Values calculated from the model range from 0.32%-10.00% (Table 1.3).

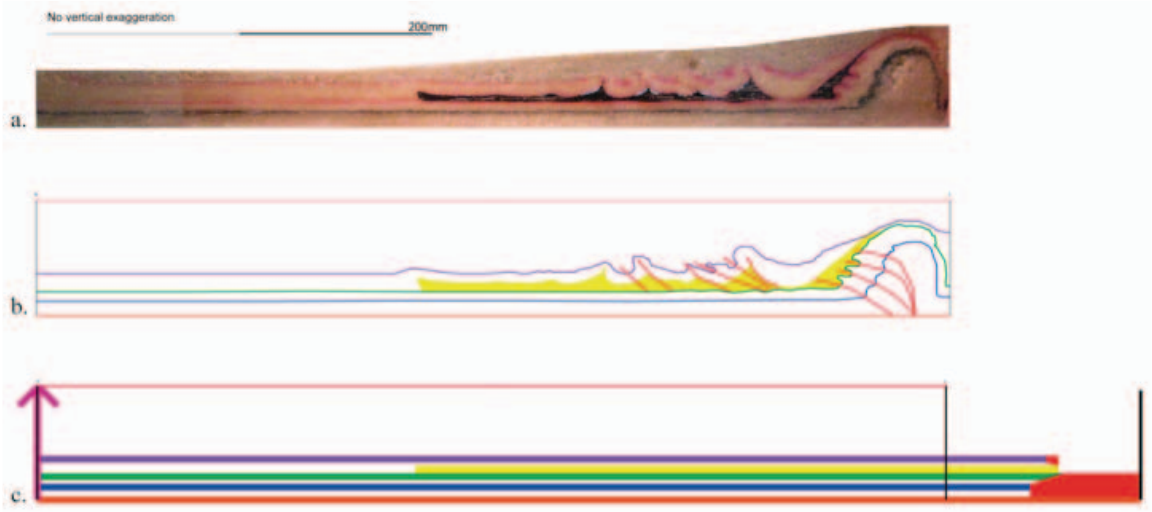

Figure 11:
a. Photograph of 18 centimeter cross-sectional cut; colors correspond to marker beds; dark, irregularly-shaped unit is the silicone polymer.
b. Line drawing of cross-section in part a.
c. Restored section where yellow corresponds to the undeformed silicone polymer cross-sectional area; red shapes denote volume lost in sequences 1 & 2.

Table 1.3: Calculated shortening across the model.

Model Slice	Horizon	Model Bulk Shortening	% Shortening from Structures	% of Total Bulk Shortening	% Shortening from LPS	% of Total Bulk Shortening
12 cm	Purple	9.70%	9.34	96.29	0.32	3.71
12 cm	Green	17.55%	10.91	62.17	6.64	37.83
12 cm	Blue	17.55%	8.79	50.09	8.75	49.91
18 cm	Purple	9.70%	8.64	89.07	1.06	10.93
18 cm	Green	17.55%	10.54	60.06	7.01	39.94
18 cm	Blue	17.55%	7.71	43.93	9.84	56.07
24 cm	Purple	9.70%	7.93	81.75	1.77	18.25
24 cm	Green	17.55%	11.2	63.82	6.35	36.18
24 cm	Blue	17.55%	7.55	43.02	10	56.98

Discussion

Layer parallel shortening values were calculated two ways: from thin sections and from analog models. LPS values from the sandbox model show less variation than results from the thin section analysis. LPS values in thin section are generally higher than values from the model.

LPS values measured from field sample thin sections range from 11.6-27.8%. These values, with the exception of sample NP2's value of 27.8%, are towards the upper limit of previously published ranges (Table 1.4). The 27.8% LPS measurement is 2.8% higher than the highest value reported in current literature (Table 1.4). The higher values (both the LPS and compaction values are highest in the sample set) described in sample

Table 1.4: LPS values from the literature.

LPS %	Citation	Measured From
2-10%	Wilschko et al. (1985)	Twinned Calcite
6%	Craddock and van der Pluijm (1989)	Twinned Calcite
10-14%	Engelder (1979)	Twinned Calcite and Pressure Solution
10%	Engelder and Engelder (1977)	Deformed Fossils and Solution Cleavage
1-21%	Whitaker and Bartholomew (1999)	Deformed Trace and Body Fossils, Chert Nodules
10-15%	Henry et al. (2003)	Anisotropy of Electrical Conductivity in Clay Rich Sediment
5-15%	Weil and Yonkee (2009)	Anisotropy of Magnetic Susceptibility (AMS)
16-23%	Sans et al. (2003)	Fissility Measurements, AMS and Strain Markers such as Burrows and Rain Drops
5-12.5%	Nilforoushan, et al. (2008)	Volume Loss in Analog Sandbox Model
17%	Koyi et al. (2004)	Bed Length in Analog Sandbox Model
18-25%	Butler and Paton (2010)	Bed Length in Analog Sandbox Model

NP2 could be due to increased stress in the center portion of the study area, original grain shapes other than ellipsoid, or a different original matrix character than the other three samples causing the rheological and mechanical properties of the sandstone to express deformation differently. One reason for this distribution is that LPS can be taken up in

different amounts for different mechanisms. Values for different measuring techniques often fall within different ranges (e.g. measuring calcite twins or deformed fossils generally yields smaller numbers; Chapple and Spang, 1974). Thin section measurements do not show a relationship with proximity to the main thrust, as no relationship between the sample and the distance to the mountain range can be generalized with confidence. However, recall that deformation decays exponentially from the collisional margin; theoretically, LPS should decline towards zero as measurements are collected away from the margin (Craddock et al., 1993).

LPS values measured from analog model cross-sections range from 0.32-10.00%, which generally fall within previously reported LPS ranges, measured in various ways (Table 1.4). Like the thin sections, there is one value that is out of the reported range: 0.32% in the uppermost purple horizon of the 12 centimeter slice. There is no appreciable difference along strike of LPS measurements except for that part of the 12 centimeter slice. Though the value of 0.32% LPS is the lowest, it follows the trend seen in all of the model slices where the purple horizon measures a much lower LPS value compared to the green and blue. This stark change is because of the two-stage nature of the model, and because of the ductile detachment. To test the LPS effects of multi-phase deformation, a model with only one phase of deformation was also run. It too showed an increase in LPS above and below the ductile detachment; however, measured values were closer together (4.12% in the purple, 4.47% in the green, and 5.71% in the blue). This relationship is not novel; it has been documented by Koyi (2004) in the Appalachians. Clearly, there is a variation in deformation accommodated by LPS as a function of the exact structures

formed. Thrust geometries change along strike in the model, and this variation in structure is thought to affect the exact amount of deformation accommodated by LPS at each point (Figure 10). Analog model LPS results show less variation than thin section measurements, and are systematically underestimating the amount of CFR shortening represented in thin section. This difference can be attributed to multiple factors. The free surface at the top of the model is predicted to decrease the amount of LPS in the system; as some of the stress is accommodated in the free-moving surface (Chapple and Spang, 1974). Another difference could be due to the two-dimensional nature of calculating LPS one cross-section at a time. Fault reactivation maintains the orientation of the original fault, and new faults form parallel that orientation, regardless of stress direction during subsequent reactivations (Dubois et al., 2002). Stress direction is not a probable source of error in the fault geometries (and thereby LPS calculations); however, there could be an element of error to the modeling process. It is important to note that LPS is measured in the sandbox model in the absence of faults as well. In a model run composed only of fine sand (i.e. without the ductile layer), LPS ranged from 5.6% in the top purple layer, to 7.2% in the blue lowermost layer. Koyi (2004) also showed that LPS increases with depth without a ductile layer. The fault cut into the two-phase model basement was made by pulling a knife through the sand. Though it was made as precisely as possible, some slant to the fault is possible. In addition, there is always an element of oblique slip to faults. Transpressional deformation within the sandbox would signify an element of strain that is missing in cross-section; any type of lateral ramp in the model would invalidate the plane strain assumption, and cause the measurements of LPS to be too low because the strain

would not be accounted for. Even though transpressional deformation is unlikely to be a factor within the model, it remains a possibility in Colorado. Each deformation event imposed on the CFR did not have the same principal stress orientation. Therefore, shortening in the CFR cross-section could be underestimated, as strike-slip motion on faults will not be expressed in cross-section.

It is important to remember key differences in data type and properties when comparing CFR thin section and analog model measurements directly. These differences lead to an underestimation in model values over measurable values from nature. First, layer parallel strain measured in thin section can be regarded as point data, where the shortening measured in the model applies to the model as a whole. Since the thin section samples were taken at points out of the main deformation front (outboard of the main thrust), the amount of LPS at that precise location may be greater than the average amount of the whole section. This hypothesis is corroborated by samples CB6 and CB3, which were collected from two adjacent formations along dip. Sample CB6, collected closer to the thrust, displays a lesser amount of LPS than sample CB3, which is farther out. This uneven expression of LPS relative to structural features is documented in the literature; for example, it has been suggested that LPS is greater in hinge zones than in the fold limbs (Chapple and Spang, 1974). Second, LPS modeled in the sandbox is fundamentally expressed differently. In this study, LPS in the CFR was measured from pressure solution shortening using the Onasch (1993) method in quartz sandstone thin sections. In the model, layer parallel deformation is not accommodated from dissolution;

it is taken up from grain packing and porosity loss as the sand is compressed. In nature, porosity loss is due to cementation and fluid movement.

Moving forward, models of increasing complexity can be run simulating the Colorado Front Range, including models that increase the study area to include the western portion of the mountain belt. More thin sections of different lithologies can be analyzed using different techniques, such as a stylolite investigation using an SEM-electron microprobe, or a microfracture analysis using cathodoluminescence. Under the premise that stylolites contain leftover material from dissolution, an investigation into stylolitic surfaces would estimate volume loss by measuring the chemical composition of the stylolite relative to the bulk rock; volume loss can be calculated based on this change in chemistry. In multiple field locations, large-scale stylolitic surfaces were expressed in outcrop by more than one per foot of vertical section. Many microstylolites accompany bed-scale stylolites, just as many microfractures accompany a fractured rock. An investigation into LPS by this method could not be found in literature. A microfracture analysis would not only yield stress directions (e.g. compaction and LPS directions), but would give information as to the timing of LPS, based on microfracture age relationships (Milliken and Laubach, 2000). Current research suggests that layer parallel deformation is pulsed, occurring at the onset of each discrete deformation event before folding and faulting occurs, but this hypothesis requires further testing (Burberry, 2013).

Conclusions

This research shows that LPS in CFR quartz arenite thin sections varies between 11.6% and 27.8%. LPS in analog models scaled to the CFR show an increase from the

top of the section downwards from 0.32% to 10%. This work suggests that LPS is accommodated throughout the deformation sequence, and not only at the onset of deformation. It further suggests that LPS and is variable both with respect to depth in the stratigraphic column and in proximity to meso- and macro-scale structures. This research also suggests that LPS is variable along strike of a deformation front. Every cross-section of the model displayed three distinct values for each horizon measured corresponding to differential LPS throughout the layers under the same applied stress. Also, values measured from field samples are variable along strike of the CFR deformation front. This suggests that LPS amounts are not predictable from known bulk shortening amounts alone, based on stratigraphic or geographic location.There is no “single solution” that is applicable to each field area. Layer parallel deformation is variable based on lithology, geologic history, and fluid movement. However, LPS can be measured; it plays a significant role in subsurface rock properties. It therefore should be an integral part of the workflow when examining compressional deformation subsurface.

Given that there is no general rule able to be applied in regards to LPS in every study area, the best practice recommendation from this research is to collect additional data to work out layer parallel shortening intricacies in each case. For example, oriented core, which is not always collected, could be partitioned into formations or mechanical stratigraphic units and LPS could be calculated using the pressure solution shortening method. LPS data could also be collected by splitting the core into areas of interest, such as source, seal, and reservoir units, when exploring for hydrocarbons. Only oriented core would work for this calculation; dip direction must be known in order to give insight into

the layer parallel deformation regime. In the ideal case, this data would allow both analog and numerical reservoir simulation models to be calibrated to include the effects of LPS appropriate to the setting being modeled.

References

Barbeau, D.L., 2003, A flexural model for the Paradox Basin: implications for the tectonics of the Ancestral Rocky Mountains: Basin Research, v. 15, p. 97-115.

Bose, S., and Mitra, S., 2010, Analog modeling of divergent and convergent transfer zones in listric normal fault systems: American Association of Petroleum Geologists Bulletin, v. 94, no. 9, p. 1425-1452.

Buiter, S.J.H., 2012, A review of brittle compressional wedge models: Tectonophysics, v. 530-531, p. 1-17.

Burberry, C.M., 2013, Identifying the amount and timing of layer parallel shortening in compressive regions using thin-sections and analog models: American Association of Petroleum Geologists Search and Discovery Article #901632013, Annual Convention and Exhibition, Pittsburgh, Pennsylvania, May 19-22, 2013.

Burberry, C.M., Nilfouroushan, F., Koyi, H.A., and Cosgrove, J.W. Modelling the effect of an upper detachment horizon on promoting triangle zone development in the Sawtooth Range, Montana, *in preparation*.

Butler, R.W.H., and Paton, D.A, 2010, Evaluating lateral compaction in deepwater fold and thrust belts: how much are we missing from “nature’s sandbox”?: GSA Today, v. 20, no. 3, p. 4-10.

Byerlee, J., 1978, Friction of Rocks: Pure and Applied Geophysics, v. 116, p. 615-626.

Cadell, H M., 1888, Experimental researches in mountain-building: Transactions of the Royal Society of Edinburgh, v. 35, 337–357.

Cerca, M., Ferrari, L., Corti, G., Bonini, M., and Manetti, P., 2010, Analogue model inversion tectonics explaining the structural diversity of Late Cretaceous shortening in southwestern Mexico: Lithosphere, v. 2, no. 3, p. 172-187.

Chapple, W.M., and Spang, J.H., 1974, Significance of layer-parallel slip during folding of layered sedimentary rocks: Geological Society of America Bulletin, v. 85, p. 1523-1534.

Craddock, J.P., Jackson, M., van der Pluijm, B.A., and Versical, R.T., 1993, Regional shortening fabrics in Eastern North America: far-field stress transmission from the Appalachian-Ouachita orogenic belt: Tectonics, v. 12, no. 1, p. 257-264.

Craddock, J.P., and van der Pluijm, B.A., 1989, Late Paleozoic deformation of the cratonic carbonate cover of eastern North America, Geology, v. 17, no. 5, p. 416-419.

Dubois, A., Odonne, F., Massonnat, G., Lebourg, T., and Fabre, R., 2002, Analogue modelling of fault reactivation: tectonic inversion and oblique remobilisation of grabens: Journal of Structural Geology, v. 24, p. 1741-1752.

Engelder, T., 1979, The nature of deformation within the outer limits of the central Appalachian foreland fold and thrust belt in New York state, Tectonophysics, v. 3-4, p. 289-310.

Engelder, T., and Engelder, R., 1977, Fossil distortion and décollment tectonics of the Appalachian plateau, Geology, v. 5, no. 8, p. 457-460.

Epard, J.-L, and Groshong Jr., R.H., 1995, Kinematic model of detachment folding including limb rotation, fixed hinges and layer-parallel strain: Tectonophysics, v. 247, p. 85-103.

Erslev, E.A., and Holdaway, S.M., 1999, Laramide faulting and tectonics of the northeastern Front Range of Colorado, *in* Lageson, D.R., Lester, A.P., and Trudgill, B.D., editors, Colorado and adjacent areas: Boulder, Geological Society of America Field Guide 1, p. 41-49.

Erslev., E.A., Kellogg, K.S., Bryant, B., Ehrlich, T.K., Holdaway, S.M., and Naeser, C.W., 1999, Laramide to Holocene structural development of the northern Colorado Front Range, *in* Lageson, D.R., Lester, A.P., and Trudgill, B.D., editors, Colorado and adjacent areas: Boulder, Geological Society of America Field Guide 1, p. 21-40.

Fischer, M.W., and Coward, M.P., 1982, Strains and folds within thrust sheets: an analysis of the Heilam sheet, northwest Scotland: Tectonophysics, v. 88, p. 291-312.

Grose, L.T., 1972, Geologic formations and structure of Colorado Springs area, Colorado: The Mountain Geologist, v. 9, p. 229-237.

Hedge, C.E., Peterman, Z.E., and Braddock, W.A., 1967, Age of the major Precambrian regional metamorphism in the northern front range, Colorado: Geological Society of America Bulletin, v. 78, no. 4, p. 551-558.

Henry, P., Jouniaux, L., Screaton, E.J., Hunze, S., and Saffer, D.M., 2003, Anisotropy of electrical conductivity record of initial strain at the toe of the Nankai accretionary prism: Journal of Geophysical Research, v. 108, doi: 10.1029/2002JB002287.

Hubbert, M.K., 1951, Mechanical basis for certain familiar geologic structures: Geological society of America bulletin, v. 62, p. 355-372.

Hubbert, M.K., 1937, Theory of scale models as applied to the study of geologic structures, Geological Society of America Bulletin, v. 48, p. 1459-1520.

Humphreys, E., 2009, Relation of flat subduction to magmatism and deformation in the western United States, *in* Kay, S.M., Ramos, V.A., and Dickinson, W.R., editors, Backbone of the Americas: shallow subduction, plateau uplift, and ridge and terrane collision: The Geological Society of America, Memoir 204, p. 85-98.

Jessup, M.J., Jones III, J.V., Karlstrom, K.E., Williams, M.L., Connelly, J.N., and Heizler, M.T., 2006, Three Proterozoic orogenic episodes and an intervening exhumation event in the Black Canyon of the Gunnison Region, Colorado: The Journal of Geology, v. 114, p. 555-576.

Jordan, T., and Allmendinger, R.W., 1986, The Sierras Pampenas of Argentina: a modern analogue of Rocky Mountain foreland deformation: American Journal of Science, v. 286, p. 737-764.

Kauffman, E.G., 1984, Paleobiogeography and evolutionary response dynamic in the Cretaceous Western Interior Seaway of North America: Geological Association of Canada Special Paper 27, p. 273-306.

Kellogg, K.S., Bryant, B., and Reed, Jr., J.C., 2004, The Colorado Front Range—anatomy of a Laramide uplift, in Nelson, E.P., and Erslev, E.A., eds., Field trips in the southern Rocky Mountains, USA: Boulder, Geological Society of America, field guide 5, p. 89-108.

Kluth, C.F., and Coney, P.J., 1981, Plate tectonics of the Ancestral Rocky Mountains: Geology, v. 9, p. 10-15.

Koyi, H., and Petersen, K., 1993, Influence of basement faults on the development of salt structures in the Danish Basin: Marine and Petroleum Geology, v. 10, p. 82-94.

Koyi, H.A., Sans, M., Teixell, A., Cotton, J., and Zeyen, H., 2004, The significance of penetrative strain in the restoration of shortened layers—insights from sand models and the Spanish Pyrenees, in McClay, K.R., editor, Thrust tectonics and hydrocarbon systems, American Association of Petroleum Geologists Memoir 82, p. 207-222.

Laubach, S.E., 1997, A method to detect natural fracture strike in sandstones: American Association of Petroleum Geologists Bulletin, v. 81, no. 4, p. 604-623.

Laubach, S.E., Olson, J.E., and Gross, M.R., 2009, Mechanical and fracture stratigraphy: American Association of Petroleum Geologists Bulletin, v. 93, no. 11, p. 1413-1426.

Milliken, K.L., and Laubach, S.E., 2000, Brittle deformation in sandstone diagenesis as revealed by scanned cathodoluminescence imaging with application to characterization of fractured reservoirs, *in* Pagel, M., Barbin, V., Blanc, P., and Ohnenstetter, D., editors, Cathodoluminescence in geosciences: Berlin, Springer-Verlag, p. 225-243.

Nilforoushan F., and Koyi, H.A., 2007, Displacement fields and finite strains in a sandbox model simulating a fold-thrust-belt: Geophysics journal international, v. 169, p. 1341-1355.

Nilforoushan, F., Koyi, H.A., Swantesson, J.O.H., and Talbot, C.J., 2008, Effect of basal friction on surface and volumetric strain in models of convergent settings measured by laser scanner: Journal of structural geology, v. 30, p. 366-379.

Oldow, J.S., Bally, A.W., Lallemant, H.G.A., and Leeman, W.P., 1989, Phanerozoic evolution of the North American Cordillera; United States and Canada, *in* Bally, A.W., and Palmer, A.R., editors, The geology of North America; an overview: Boulder, Geological Society of America, v. A, p. 139-232.

Onasch, C.M., 1993, Determination of pressure solution shortening in sandstones, Tectonophysics, v. 227, p. 145-159.

Ricker, N., 1941, A note on the determination of the viscosity of shale from the measurement of wavelet breadth: Geophysics, v. 6, no. 3, p. 254-258.

Ross, C.A., 1979, Late Paleozoic collision of North and South America: Geology, v. 7, p. 41-44.

Sans, M., Vergés, J., Gomis, E., Parés, J.M., Schiattarella, M., Travé, A., Calvet, F., Santanach, P., and Doulcet, A, 2003, Layer parallel shortening in salt-detached folds: constraint on cross-section restoration: Tectonophysics, v. 372, p. 85-104.

Schellart, W.P., 2000, Shear test results for cohesion and friction coefficients for different granular materials: scaling implications for their usage in analogue modelling: Tectonophysics, v. 324, p. 1-16.

Schreurs, G., Buiter, S.J.H., Boutelier, D., Corti, G., Costa, E., Cruden, A.R., Daniel, J., Hoth, S., Koyi, H.A., Kukowski, N., Lohrmann, J., Ravaglia, A., Schlische, R.W., Withjack, M.O., Yamada, Y., Cavozzi, C., Del Ventisette, C., Brady, J.A.E., Hoffmann-Rothe, A., Mengus, J., Montanari, D., and Nilforoushan, F., 2006, Analogue benchmarks of shortening and extension experiments, *in* Buiter, S.J.H., and Schreurs, G., editors, Analogue and numerical modelling of crustal-scale processes: London, Geological Society of London Special Publication, v., 253, p. 1-27.

Smith, D.R., Noblett, J, Wobus, R.A., Unruh, D., and Chamberlain, K., 1999, A review of the Pikes Peak batholith, Front Range, central Colorado: a “type example” of A-type granitic magmatism: Rocky Mountain Geology, v. 34, no. 2, p. 289-312.

Steven, T.A., Evanoff, E., and Yuhas, R.H., 1997, Middle and Late Cenozoic tectonic and geomorphic development of the Front Range of Colorado: Rocky Mountain Association of Geologists Colorado Front Range Guidebook, p. 115-124.

Sweet, D.E., and Soreghan, G.S., 2010, Late Paleozoic tectonics and paleogeography of the ancestral Front Range: structural, stratigraphic, and sedimentologic evidence from the Fountain Formation (Manitou Springs, Colorado): Geological Society of America Bulletin, v. 122, no. 3, p. 575-594.

Turrini, C., Ravaglia, A., and Perotti, C.R., 2001, Compressional structures in a multilayered mechanical stratigraphy: insights from sandbox modeling with three-dimensional variations in basal geometry and friction, *in* Koyi, H.A., and Mancktelow, N.S., editors, Tectonic modeling: a volume in honor of Hans Ramberg: Boulder, Geological Society of America Memoir 193, p. 153-178.

Tweto, O., compiler, 1979, Geologic map of Colorado: U.S. Geological Survey of Colorado, scale 1:500,000, 2 sheets.

Tweto, O., 1980a, Precambrian geology of Colorado, *in* Kent, H.C., and Porter, K.W., editors, Colorado geology: Denver, Rocky Mountain Association of Geologists 1980 Symposium, p. 37-45.

Tweto, O., 1980b, Summary of Laramide orogeny in Colorado, *in* Kent, H.C., and Porter, K.W., editors, Colorado geology: Denver, Rocky Mountain Association of Geologists 1980 Symposium, p. 129-134.

Tweto, O., 1980c, Tectonic history of Colorado, *in* Kent, H.C., and Porter, K.W., editors, Colorado geology: Denver, Rocky Mountain Association of Geologists 1980 Symposium, p. 5-9.

Weijermars, R., 1992, Progressive deformation in anisotropic rocks: Journal of Structural Geology, v. 14, no. 6, p. 723-742.

Weil, A.B., and Yonkee, A., 2009, Anisotropy of magnetic susceptibility in weakly deformed red beds from the Wyoming salient, sevier thrust belt: relations to layer-parallel shortening and orogenic curvature: Lithosphere, v. 1, no. 4, p. 235-256.

Weimer, R.J., and Le Roy, L.W., 1987, Paleozoic-Mesozoic section: Red Rocks Park, I-70 road cut, and Rooney Road, Morrison area, Jefferson County, Colorado: Geological Society of America Centennial Field Guide--Rocky Mountain Section, p. 315-319.

Whitaker, A.E., and Bartholomew, M.J., 1999, Layer parallel shortening: a mechanism for determining deformation timing at the junction of the central and southern Appalachians: American Journal of Science, v. 299, p. 238-254.

Wiltschko, D.V., Medwedeff, D.A., and Millson, H.E., 1985, Distribution and mechanisms of strain within rocks on the northwest ramp of Pine Mountain block, southern Appalachian foreland: a field test of theory, Geological Society of America Bulletin, v. 96, p. 426-435.

Withjack, M.O., and Schlische, R.W., 2006, Geometric and experimental models of extensional fault-bend folds: Geological Society of London Special Publication no. 253, p. 2885-305.

APPENDIX A

Additional samples used in thin section analysis:

NP2

a.

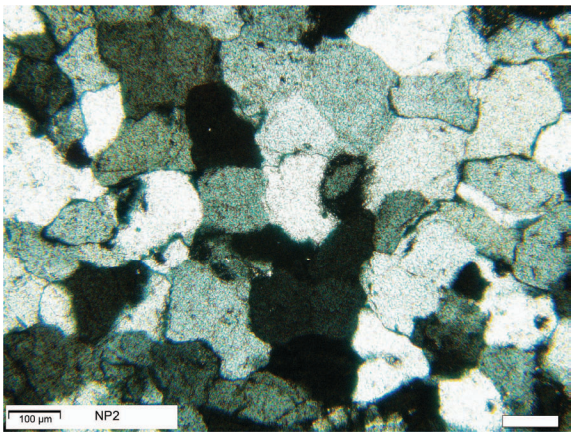

b.

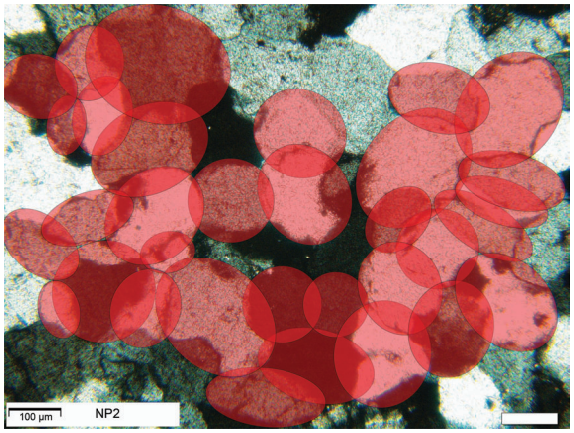

c.

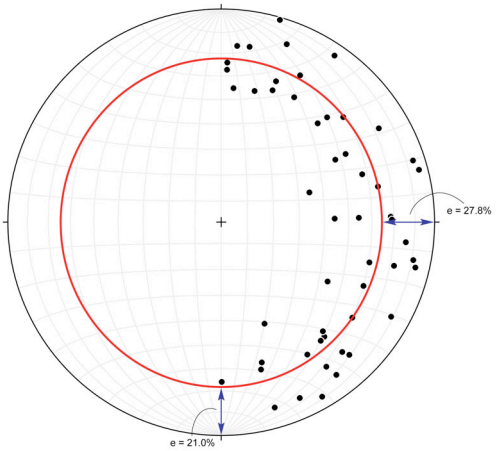

Analysis of sample NP2 utilizing the Onasch (1993) method.
a. Photomicrograph under cross-polarized light.
b. Photomicrograph with best fit ellipses drafted on.
c.S tereonetof pl ottedl ayerpa rallels horteninga nd compaction directions.

CB6

a.

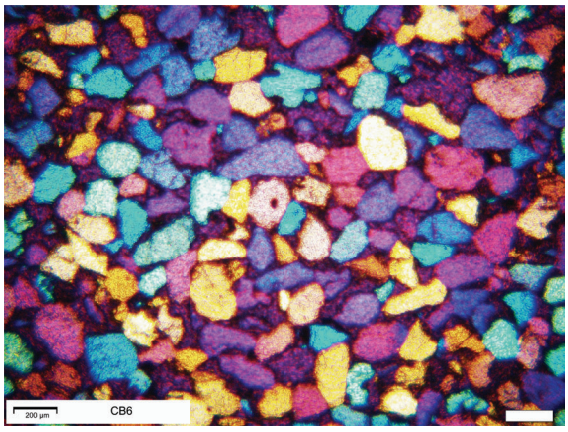

b.

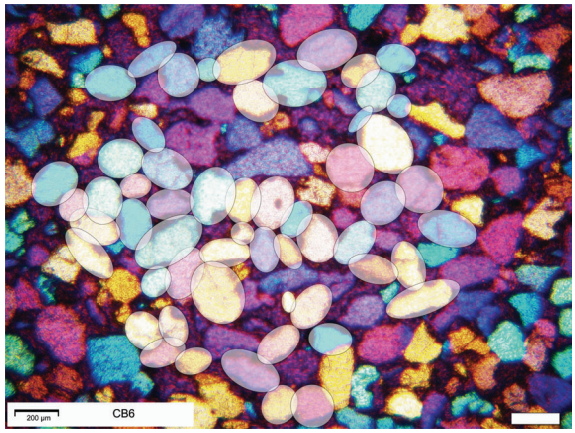

c.

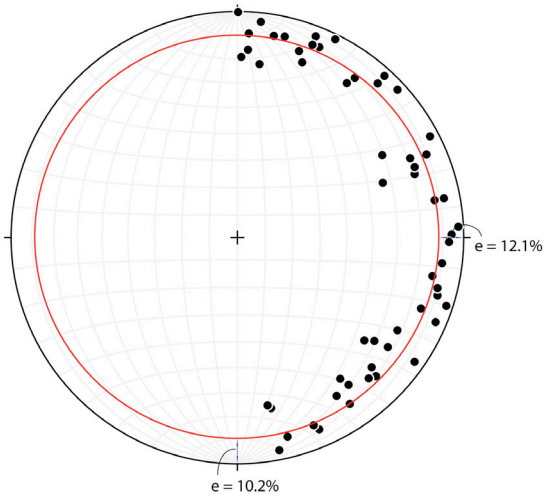

Analysis of sample CB6 utilizing the Onasch (1993) method.
a. Photomicrograph under cross-polarized light with the gypsum plate in.
b. Photomicrograph with best fit ellipses drafted on.
c. Stereonet of plotted layer parallel shortening and compaction directions.

NP6

a.

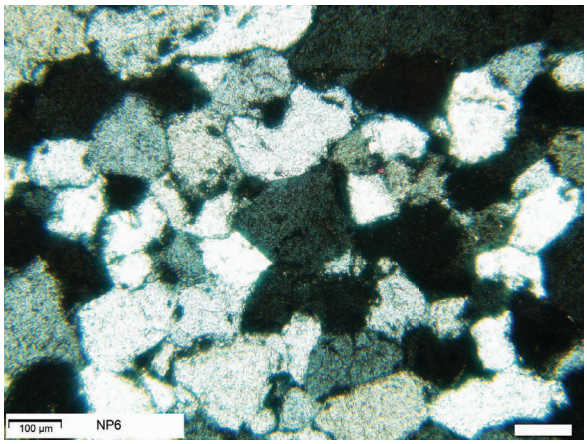

b.

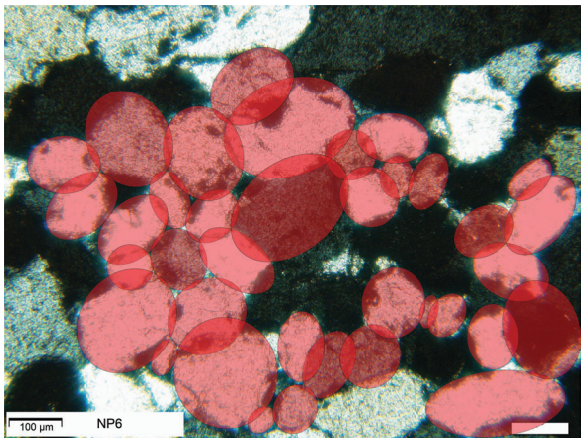

c.

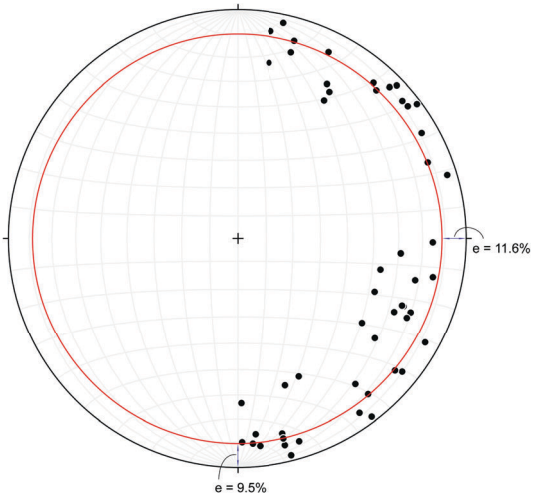

Analysis of sample NP6 utilizing the Onasch (1993) method.
a. Photomicrograph under cross-polarized light.
b. Photomicrograph with best fit ellipses drafted on.
c.S tereonetof pl ottedl ayerpa rallels horteninga nd compaction directions.